Measurement of oscillator strength distribution in the discrete and continuous spectrum of lithium

Shahid Hussain, M. Saleem, and M. A. Baig*
Atomic and Molecular Physics Laboratory, Department of Physics, Quaid-i-Azam University, Islamabad 45320, Pakistan
(Received 13 November 2006; published 12 February 2007)

The oscillator strength distribution in the discrete and continuous regions of the spectrum of lithium has been determined by employing the saturation technique in conjunction with a thermionic diode ion detector. The photoionization cross section from the $3s\ ^2S$ excited state at the ionization threshold has been determined by the direct absorption of the 614 nm laser and also from extrapolating the photoabsorption cross sections measured for eight transitions of the $3s\ ^2S \rightarrow np\ ^2P$ ($n=14,16,18,20,22,24,26,28$) Rydberg series. The average value of the photoionization cross section measured at the ionization threshold has been used to extract the f values for the $3s\ ^2S \rightarrow np\ ^2P$ Rydberg series of lithium from $n=14$ to $n=56$. The measured f values of the observed Rydberg series decrease smoothly with an increase of the principal quantum number. The oscillator strength densities in the continuum region have also been determined from the measured values of the photoionization cross section from the $3s\ ^2S$ excited state at four ionizing laser wavelengths above the first ionization threshold. Continuity has been found between the discrete and the continuous spectrum across the ionization threshold.

DOI: 10.1103/PhysRevA.75.022710 PACS number(s): 32.80.Fb, 32.80.Rm, 32.80.Cy

I. INTRODUCTION

The measurement of the oscillator strength and that of the photoionization cross section is a subject of considerable interest for many fields. The photoionization is the simplest process giving detailed information on the atomic and molecular structure. The oscillator strengths are very important in astrophysical studies because they play a significant role in the determination of the atomic abundance. They are also important in the studies of controlled thermonuclear reactions. The distribution of the dipole oscillator strength as a function of excitation energy is an important property of an atom or molecule [1]. In the discrete region the oscillator strength distribution directly determines the photoabsorption cross sections and governs the refractive index and other optical properties of the material whereas, this distribution in the continuum yields the absolute value of the photoionization cross section.

Different experimental techniques have been used for the determination of oscillator strengths such as through emission, absorption, or dispersion measurements or via combined measurements of branching ratio and lifetimes [2]. Huber and Sandeman [3] reviewed the various techniques of the oscillator strength measurements and also discussed the merits and demerits of these techniques. Limited literature is available about the optical oscillator strength data, because most of the available measuring methods have some limitations, which restrict their range of applications [4]. Filippov [5] determined the relative oscillator strength for the $2s \rightarrow np$ ($3 \leqslant n \leqslant 13$) Rydberg series of lithium by the anomalous dispersion measurements. Marr and Greek [6] performed an analysis of the available data on the oscillator strengths for the principal series and the associated photoionization continuum for each of the alkali metal atoms. Wiese and Wiese [7] studied the regularities and systematic trends among the atomic oscillator strengths giving numerical examples of several atoms including lithium. Martin and Wiese [8] described an analysis yielding the oscillator strength distributions in several spectral series throughout the lithium isoelectronic sequence. Subsequently, Martin and Wiese [9] critically evaluated and compiled the oscillator strengths of the lithium isoelectronic sequence for the transitions of types $ms \rightarrow np$, $mp \rightarrow ns$, and $mp \rightarrow nd$ ($2 \leqslant m \leqslant 4$ and $3 \leqslant n \leqslant 7$). Sims *et al.* [10] calculated the oscillator strengths for the $1s^2\ ns\ S^2 \rightarrow 1s^2\ mp\ ^2P$ ($n,m=2,3,4,5$) transitions of lithium. Amusia and Cherepkov [11] calculated the photoionization cross sections and the oscillator strengths for helium, lithium, and beryllium in the framework of the random-phase approximation with exchange (RPAE). Hofsaess [12] calculated the photoionization cross sections and oscillator strengths for the principal series of alkali metals. Subsequently, Martin and Barrientos [13] computed the oscillator strengths for the alkali group of elements using quantum defect orbital (QDO) formalism. Barrientos and Martin [14] obtained the oscillator strength distribution between the discrete and continuous spectra of the alkali elements by following the quantum defect orbital procedure. Barrientos and Martin [15] calculated the oscillator strengths for the sharp and diffuse series of the alkali metal atoms using the quantum defect orbital method including the core-polarization effects. Peach *et al.* [16] calculated the bound state energies, oscillator strengths, and photoionization cross sections for the members of lithium isoelectronic sequence. Barrientos and Martin [17] discussed the dependence of f values on the reciprocal of the nuclear charge in lithium isoelectronic sequence. Hollauer and Nascimento [18] calculated the photoionization cross sections, oscillator strengths, and dynamic polarizabilities for the lithium atom and its positive ion using a discrete basis set to represent both the bound and the continuum states. The oscillator strength for the $2\ ^2S \rightarrow 2\ ^2P$ transition has been extensively studied [19–23] and a high

*Corresponding author. Email address: baig@qau.edu.pk

precision results have been obtained. The most accurate oscillator strengths for $2\,^2S \rightarrow 2^2P$ and $2\,^2P \rightarrow 3\,^2D$ transitions were given by Yan and Drake [22]. Qu *et al.* [24] obtained the discrete oscillator strengths for the $1s^2 2\ s \rightarrow 1s^2\ np$ $(3 \leqslant n \leqslant 9)$ transitions of the lithium isoelectronic sequence up to $Z=10$ using a full core plus correlation (FCPC) method. They also calculated the oscillator strength densities corresponding to the bound-free transitions. No experimental as well as theoretical data are available for the high lying transitions of the $3s\,^2S \rightarrow np\,^2P$ $(3 \leqslant n \leqslant \text{limit})$ Rydberg series except for a few lower members of the series [9,16].

In this work, we present experimental determination of the optical oscillator strengths in the discrete and continuous regions of lithium spectrum using $3s\,^2S$ as an intermediate state. The photoionization cross section at the ionization threshold have been determined by the direct absorption of the 614 nm laser radiation as well as by extrapolating the cross sections measured at eight Rydberg transitions below the first ionization threshold. The average value of the measured cross section at the threshold has been used to extract the f values of the $3s\,^2S \rightarrow np\,^2P$ $(14 \leqslant n \leqslant 56)$ Rydberg series of lithium. Four different regions of the continuum, above the first ionization threshold, have also been investigated at the ionizing wavelengths of 532 nm, 440 nm, 355 nm, and 266 nm corresponding to the excess energy of 0.3 eV, 0.8 eV, 1.5 eV, and 2.6 eV, respectively. The density of the oscillator strength has also been deduced from these measured values of the photoionization cross sections and continuity has been found across the ionization threshold.

II. EXPERIMENTAL SET-UP

A schematic of the experimental arrangement for the measurement of the dipole oscillator strength distribution using the $3s\,^2S$ excited state of lithium is shown in Fig. 1. The laser system comprised of a Q-switched pulsed Nd: YAG laser (Brilliant B, Quantel) coupled with the SHG and the THG modules for producing lasers at wavelengths 532 nm and 355 nm, capable of delivering energies 450 mJ and 200 mJ, respectively. It operates at 10 Hz with pulse duration of $\approx$5 ns. The 90% of the laser energy at 532 nm was used to pump a commercial dye laser system (Quantel, TDL-90) while the remaining 10% was used to pump a homemade Hanna type [25] dye laser. The cavity of this dye laser was formed between a flat mirror and a 2400 lines/mm holographic grating and the wavelength tuning was achieved by rotating the grating with a computer controlled stepper motor. The dye laser wavelength was constantly monitored by a spectrometer (Ocean Optics, HR2000) equipped with a 600 lines/mm grating.

The lithium vapors were produced in a thermionic diode ion detector composed of a stainless steel tube 48 cm long, 3 cm in diameter and 1 mm wall thickness. About 20 cm of the central part of the tube was placed in a clamp-shell oven. Both ends of the tube were water-cooled and sealed with 25 mm diameter quartz windows. The thermionic diode was then heated up to 800 K corresponding to a lithium vapor pressure of $\approx$0.01 Torr. The temperature was monitored by a Ni-Cr-Ni thermocouple and it was maintained within $\pm 1\%$

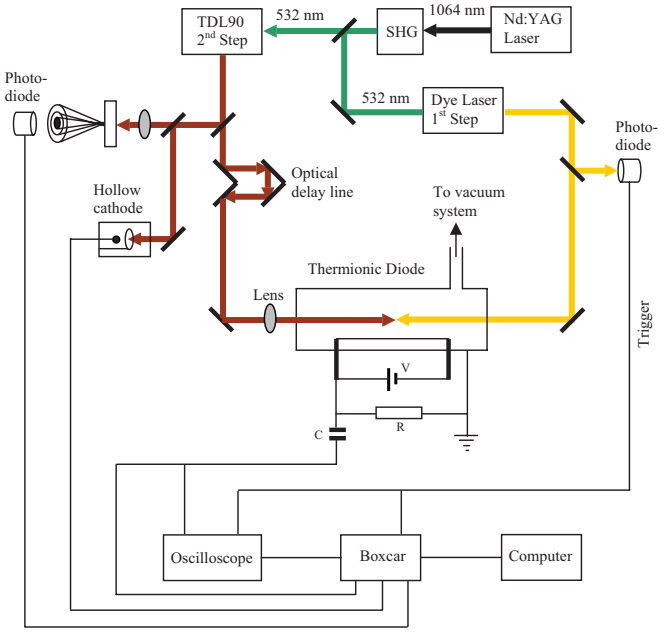

FIG. 1. (Color online) A schematic diagram of the experimental setup for the two-step photoionization of lithium.

by a temperature controller. A molybdenum wire 0.25 mm in diameter stretched axially was heated by a separate regulated dc power supply that served as a cathode for the ion detection. About 2 g of spectroscopically pure natural lithium was placed at the center of the thermally heated zone of the tube. The tube was evacuated up to 10^{-6} Torr and subsequently filled with argon gas at a pressure of about 0.2 Torr. Argon serves as a buffer gas that provides a uniform column of lithium vapors and also protects the quartz windows from the metallic coatings.

The homemade dye laser pumped by the 532 nm laser, charged with Pyradine-2 dissolved in PC (Propylene Carbonate) and tuned at 735.1 nm was used to populate the $3s\,^2S$ excited state via two-photon excitation. The excited atoms were then ionized by the lasers at wavelengths 532 nm (second harmonic), 355 nm (third harmonic), 266 nm (fourth harmonic) of the Nd:YAG laser and at 440 nm. The ionizing wavelength at 440 nm was achieved by charging the TDL-90 dye laser with the Coumarin 440 dye dissolved in methanol and pumped with the THG of the Nd:YAG laser. The ionization signals were registered as a change in the voltage across a 100 kΩ load resistor. The intensity of the ionizing laser was varied by inserting the neutral density filters (Edmund Optics) and on each insertion the energy was measured by an energy meter (R-752, Universal Radiometer). The variation in the amplitude of the ionization signal with the laser intensity was recorded using a 200 MHz digital storage oscilloscope (TDS 2024) and a computer through RS232 interface.

The $3s\,^2S \rightarrow np\,^2P$ $(14 \leqslant n \leqslant 56)$ Rydberg series was recorded by charging the dye laser TDL-90 with the DCM dye dissolved in methanol. The wavelength calibration was achieved by recording simultaneously the output from the thermionic diode, the optogalvanic spectra of neon from a hollow cathode lamp and rings from a 1 mm thick fused silica Fabry-Perot etalon (FSR 3.33 cm^{-1}) via three boxcar

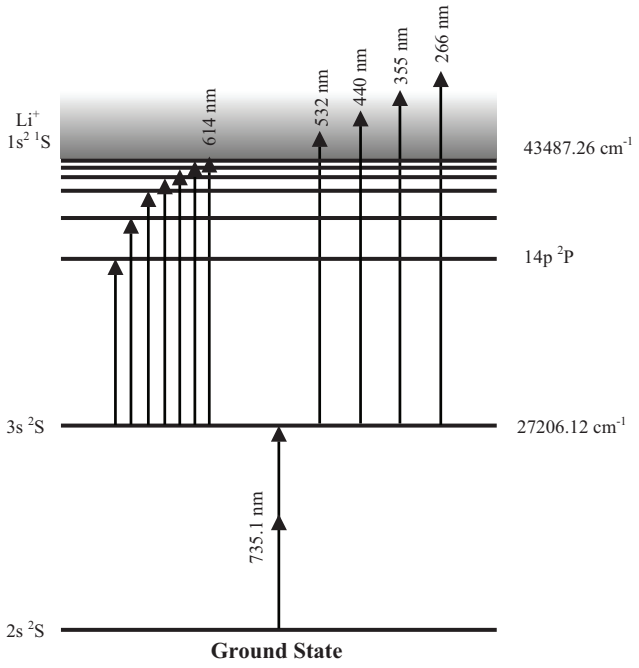

FIG. 2. (Color online) Energy level diagram for the measurements of the oscillator strengths for the $3s\,^2S \rightarrow np\,^2P$ $(14 \leqslant n \leqslant 56)$ transitions of lithium.

averagers (SR 250). The optogalvanic signals from the neon hollow cathode lamp provided well distributed spectral lines of neon in the region of interest, listed in the MIT Table [26], that serve as wavelength standards. The interference fringes from the etalon were used to interpolate between the neon lines. The spectrum was recorded with a 0.05 cm^{-1} scanning step of the dye laser. From the location of the peak signal positions, the transition energies have been determined within an accuracy of ± 0.2 cm^{-1}.

The line width of the Hanna type dye laser was $\leqslant 0.3$ cm^{-1} while that of the TDL-90 it was $\leqslant 0.1$ cm^{-1}. Both the laser pulses were linearly polarized with parallel polarization axis. The two laser beams (the exciting and the ionizing) enter the thermionic diode from the opposite sides and overlap at its center. The temporal overlap of both the laser pulses was checked using a fast PIN photodiode (BPX 65). The relative delay between the exciter and the ionizer laser pulses was controlled and varied by an optical delay line.

III. RESULTS AND DISCUSSION

The two-step excitation/ionization scheme for the measurement of the optical oscillator strength distribution in the discrete and continuous spectrum of lithium is shown in Fig. 2. The absolute oscillator strength for the high lying members of the $3s\,^2S \rightarrow np\,^2P$ Rydberg series have been determined with the experimental technique developed by Mende and Kock [27], who obtained a simple relation between the f values of the Rydberg transitions and the photoionization cross section measured at the ionization threshold as

$$f_n = \frac{4\varepsilon_o mcS_n\lambda_{1+}}{e^2 S_{1+}\lambda_n}\sigma^{1+}. \tag{1}$$

Here f_n is the oscillator strength for the nth transition of a Rydberg series, which is directly proportional to the photoionization cross section σ^{1+} measured at the threshold ionizing wavelength λ_{1+}. The quantity S_{1+} is the ion signal at the ionization threshold and S_n is the integrated ion signal intensity for the nth transition. Also the constants m, e, c, and ε_o are the mass of electron, the charge on electron, speed of light, and the permittivity of free space, respectively.

The photoionization cross section σ^{1+} from the $3s\,^2S$ excited state of lithium at the ionization threshold have been determined using the saturation technique as described by Burkhardt *et al.* [28,30], He *et al.* [29], and Saleem *et al.* [30]. This technique has been widely used for the measurement of the photoionization cross sections of the excited states of alkali, alkaline earths, and rare gas atoms ([28–33] and references therein). We have already extended this technique for the measurement of photoionization cross sections and optical oscillator strengths of the auto-ionization resonances in neon using a hollow cathode dc discharge [34]. Recently, we have applied the saturation method to determine the photoionization cross sections of the excited states of the helium [32] in a dc discharge and that of lithium [35] using the thermionic diode ion detector. The photoions produced as a result of two-step photoionization process are detected as a voltage across the load resistor. The collected charge Q per pulse in terms of this voltage signal is

$$Q = \left(\frac{(\text{voltage signal})}{R}\right)\Delta t. \tag{2}$$

Here R is the load resistance and Δt is the FWHM pulse width of the photoion signal peak in seconds.

In the absence of collisions and ignoring the spontaneous emission, for a pure two step photoionization process the rate equations have been solved to find a relation between the total charge "Q" per pulse and the photoionization cross section [28] as

$$Q = eN_0V_{vol}\left[1 - \exp\left(-\frac{\sigma U}{2\hbar\omega A}\right)\right]. \tag{3}$$

Here e is the electronic charge, N_0 is the density of the excited atoms, A is the cross sectional area of the ionizing laser beam, U is the total energy per pulse of the ionizing laser; V_{vol} is the interaction volume, and σ is the absolute cross section for photoionization. This equation holds with the assumption that the intensity of the ionizing laser is much higher, i.e., in access to that required for saturating the resonance transition; also the transition remain saturated during the laser pulse and the laser beam is uniform and linearly polarized. The accurate measurement of the photoionization cross section σ requires accurate measurement of the ionizing laser energy as well as the characterization of the spatial profiles of both the exciting and the ionizing laser pulses in the interaction region. The uncertainty in the energy determination is mainly due to the energy fluctuations in the Nd:YAG laser $(\pm 5\%)$ and in the measuring instrument

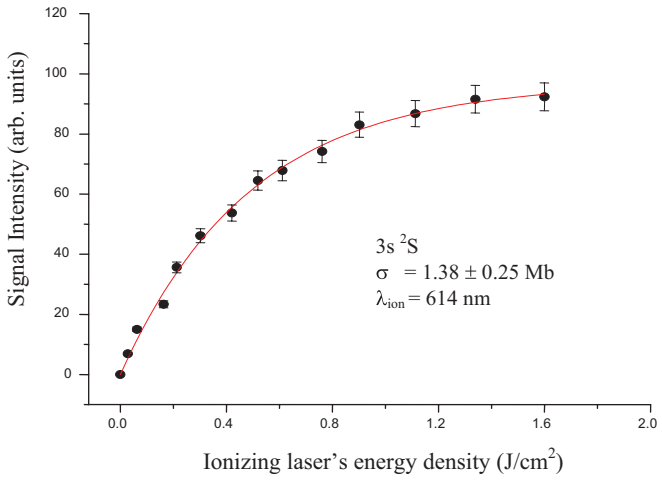

FIG. 3. (Color online) The photoionization data for the $3s\,^2S$ excited state of lithium at the ionization threshold with the ionizing laser set at 614 nm. The solid line is the least squares fit to Eq. (3) to the observed data for extracting the photoionization cross section. The error limits on the data results from pulse-to-pulse fluctuations in the signal.

(±3%). To characterize the spatial profiles of the exciting and the ionizing lasers, two beam splitters were placed before the entrance of the thermionic diode and small fractions of the laser beams were used to reproduce their spatial profiles at the interaction region. The spatial profiles of the laser beams were generated by scanning a PIN photodiode across their diameters. The intensity distribution of both the laser beams were found to be Gaussian and their spot sizes were determined at the point where the irradiance (intensity) falls to $1/e^2$ of their axial values. The diameter of the exciting laser was ≈3 mm, which passes through the center of the thermionic diode ion detector. An aperture was placed in the path of the ionizing laser to confine its diameter to ≈2 mm. Since the diameter of the ionizing laser beam was smaller than that of the exciting laser, it therefore reduces the problems associated with the spatial overlap of the beams. A lens of 50 cm focal length was used in the path of the ionizing laser to meet the power requirements for saturation. The area of the overlap region in the confocal limit was calculated using the following relation [36,37]

$$A = \pi\omega_0^2\left[1 + \left(\frac{\lambda_{io} z}{\pi\omega_0^2}\right)^2\right]. \tag{4}$$

Here "z" is the distance on the beam propagation axis from the focus and $\omega_0 = f\lambda_{io}/\pi\omega_s$ is the beam waist at $z=0$, ω_s is half the spot size of the ionizing laser beam on the focusing lens, f is the focal length, and λ_{io} is the wavelength of the ionizing laser.

The $3s\,^2S$ excited state have much greater lifetime ($\tau(3s) \approx 30.2$ ns [38]) than the pulse width (≈5 ns) of both the exciting and the ionizing lasers. Therefore, in order to separate the excitation and the ionization steps and to ensure a pure two-step photoion signal the ionizing laser was delayed by ≈5 ns. The linearity of the thermionic diode ion detector is very important while recording the experimental data of the photoionization signals so that an actual change of the photoions signal verses the energy density of the ionizing laser can be registered. We configured the linearity of our detector for the strongest photoion signal corresponding to the maximum available ionizing laser intensity. Collisional ionization due to the buffer gas atoms is the dominant process in a thermionic diode [39]. We have optimized the oven temperature and the buffer gas pressure such that the ionization probability for Rydberg states with $n \geqslant 14$ approaches to

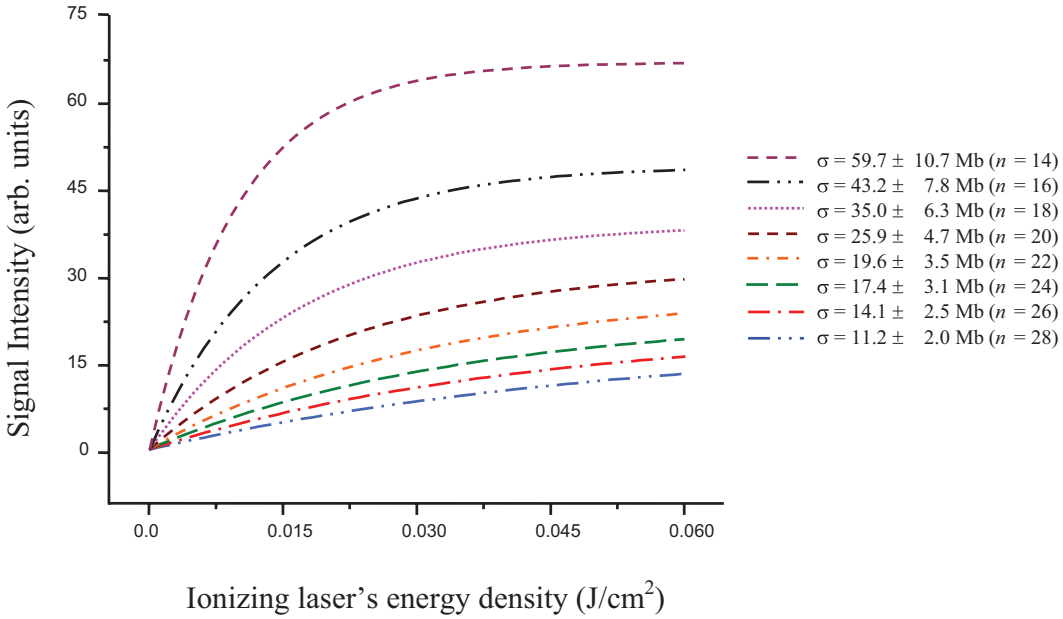

FIG. 4. (Color online) The fitted curves to the experimental data verses the energy density of the ionizing laser for eight transitions of the $3s\,^2S \rightarrow np\,^2P$ (n=14,16,18,20,22,24,26,28) Rydberg series of lithium. These fitted curves are used to extract the photoabsorption cross sections for the eight Rydberg transitions.

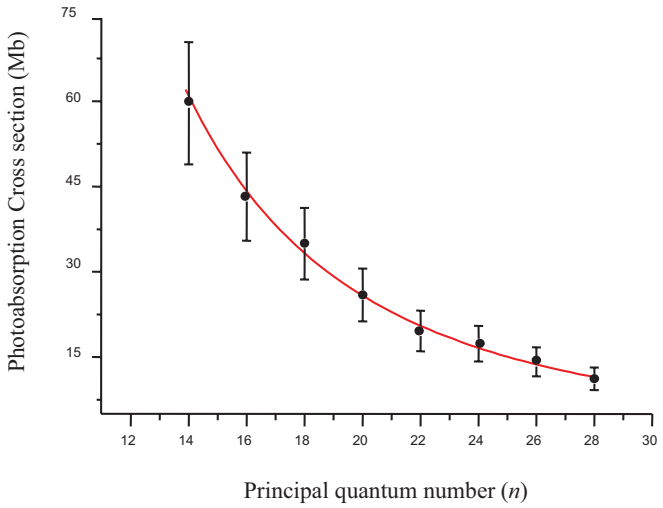

FIG. 5. (Color online) A plot of the photoabsorption cross section for the eight transitions of the $3s\,^2S \rightarrow np\,^2P$ ($n=14,16,18,20,22,24,26,28$) Rydberg series of lithium versus the principal quantum number n. The solid line which passes through the data points is fit to Eq. (5).

one [40], which is a necessary condition for using Eq. (1). In addition, the energy difference between the first ionization threshold and the $n=14$ Rydberg level is ≈ 0.07 eV whereas the value of kT (thermal energy) for the present experimental conditions is also ≈ 0.07 eV. This further complements the maximum ionization efficiency of the Rydberg states with $n \geqslant 14$.

In order to determine the photoionization cross section at the first ionization threshold the lithium atoms were first excited to the $3s\,^2S$ state via two-photon excitation from the ground state and then promoted to the ionization continuum using the 614 nm laser wavelength. The energy of the ionizing laser was then varied by inserting the neutral density filters in its path. The variation in the amplitude of the photoion signals, produced as a result of this two-step process, was plotted as a function of the intensity of the ionizing laser. A typical experimental curve for the photoionization of $3s\,^2S$ excited state of lithium at the first ionization threshold is presented in Fig. 3. The solid line that passes through the experimental data points is the least square fit to Eq. (3). It is evident that the photoion signal first increases linearly with the ionizing laser's intensity and then saturates, i.e., the photoion signal stops to increase by a further increase in the ionizing laser intensity. The photoionization cross section from the $3s\,^2S$ excited state at the ionization threshold, measured from this fitting procedure, is 1.38 ± 0.25 Mb.

The threshold photoionization cross section from the $3s\,^2S$ excited state has also been determined by extrapolating the photoabsorption cross sections measured for eight transitions of the $3s\,^2S \rightarrow np\,^2P$ ($n=14,16,18,20,22,24,26,28$) Rydberg series (see Fig. 2). The photoabsorption cross sections for these eight Rydberg transitions were measured using the saturation method as described above. The photoion signal as a function of the intensity of the second laser, for the eight Rydberg transitions, are plotted in Fig. 4. Each curve is the least square fit of Eq. (3) to the experimental

TABLE I. Term energies and the oscillator strengths for the $3s\,^2S \rightarrow np\,^2P$ Rydberg series of lithium.

n	n^*	Wavelength (nm)	Oscillator strength ($\pm 20\%$)
14	13.958	636.24	7.411×10^{-5}
15	14.954	633.30	5.197×10^{-5}
16	15.953	630.92	4.624×10^{-5}
17	16.956	628.96	3.660×10^{-5}
18	17.948	627.33	3.983×10^{-5}
19	18.953	625.95	3.329×10^{-5}
20	19.949	624.79	2.481×10^{-5}
21	20.957	623.79	2.760×10^{-5}
22	21.958	622.92	1.931×10^{-5}
23	22.949	622.17	1.954×10^{-5}
24	23.950	621.34	1.792×10^{-5}
25	24.949	620.76	1.531×10^{-5}
26	25.946	620.25	1.458×10^{-5}
27	26.945	619.79	1.116×10^{-5}
28	27.955	619.39	1.045×10^{-5}
29	28.951	619.02	9.211×10^{-6}
30	29.939	618.69	1.117×10^{-5}
31	30.954	618.39	7.958×10^{-6}
32	31.954	618.12	8.123×10^{-6}
33	32.953	617.88	5.644×10^{-6}
34	33.954	617.65	6.480×10^{-6}
35	34.957	617.45	7.284×10^{-6}
36	35.955	617.26	5.858×10^{-6}
37	36.965	617.09	5.179×10^{-6}
38	37.958	616.93	5.067×10^{-6}
39	38.963	616.78	5.334×10^{-6}
40	39.965	616.64	4.390×10^{-6}
41	40.957	616.52	4.048×10^{-6}
42	41.960	616.40	3.895×10^{-6}
43	42.952	616.29	3.506×10^{-6}
44	43.936	616.19	3.435×10^{-6}
45	44.968	616.10	3.569×10^{-6}
46	45.984	616.00	3.007×10^{-6}
47	46.987	615.92	2.922×10^{-6}
48	47.974	615.84	2.510×10^{-6}
49	48.968	615.77	2.560×10^{-6}
50	49.979	615.70	2.133×10^{-6}
51	50.980	615.64	1.948×10^{-6}
52	51.953	615.57	1.982×10^{-6}
53	52.969	615.52	1.919×10^{-6}
54	53.953	615.46	2.023×10^{-6}
55	54.986	615.41	1.804×10^{-6}
56	55.973	615.36	1.587×10^{-6}

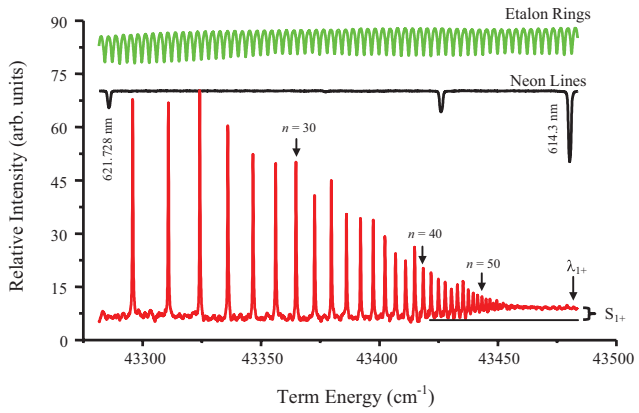

FIG. 6. (Color online) A portion of the $3s\,^2S \rightarrow np\,^2P$ ($24 \leqslant n \leqslant 56$) Rydberg series of lithium.

data points. It is evident that for a higher value of the cross section, the photoion signal gets saturated at a lower intensity.

The photoabsorption cross sections for the above mentioned eight Rydberg transitions of the $3s\,^2S \rightarrow np\,^2P$ Rydberg series, determined from the fitting procedure, plotted against the corresponding principal quantum number are shown in Fig. 5. The solid line that passes through the experimental data points is the least square fit to an expression

$$\sigma = K(n)^{-\alpha}. \tag{5}$$

Here σ is the photoabsorption cross section; K and α are constants. The value of α turns out to be 2.4 for the eight transitions of the $3s\,^2S \rightarrow np\,^2P$ Rydberg series. The measured values of the photoabsorption cross section were then extrapolated to get the photoionization cross section of the $3s\,^2S$ excited state at the first ionization threshold. This procedure yields the value of the photoionization cross section from the $3s$ excited state as 1.25 ± 0.23 Mb at the ionization threshold whereas the direct photoionization from the $3s$ excited state at the threshold is 1.38 Mb. The average value of the photoionization cross section (1.32 ± 0.24 Mb) at the threshold, measured from two different procedures, was then used to extract the f values of the $3s\,^2S \rightarrow np\,^2P$ Rydberg series. The measured value (1.32 ± 0.24 Mb) of the threshold cross section is in excellent agreement with the theoretical work of Aymar *et al.* [41] (1.48 Mb), Moskvin [42] (1.27 Mb), Ya'akobi [43] (1.42 Mb), Gezalov and Ivanova [44] (1.17 Mb), Caves and Dalgarno [45] (1.42 Mb).

Besides, we have recorded the $3s\,^2S \rightarrow np\,^2P$ ($14 \leqslant n \leqslant 56$) Rydberg series of lithium to determine the values of the remaining parameters λ_n, λ_{1+}, S_{1+}, and S_n used in Eq. (1). A portion of the recorded Rydberg series from $n=24$ to $n=56$ is shown in Fig. 6. The top trace is the etalon fringes and the middle trace is the wavelength calibration spectrum of neon. The values of the absolute oscillator strength for the $3s\,^2S \rightarrow np\,^2P$ Rydberg transitions from $n=14$ to $n=56$ were then evaluated with the help of Eq. (1). The extracted values of the oscillator strengths along with the corresponding wavelengths, the effective principal quantum number (n^*) and the associated quantum defects for the $3s\,^2S \rightarrow np\,^2P$

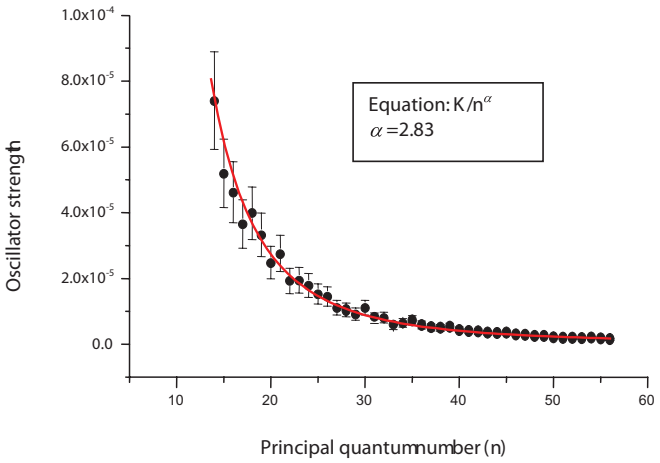

FIG. 7. (Color online) A plot of the optical oscillator strengths of the $3s\,^2S \rightarrow np\,^2P$ ($14 \leqslant n \leqslant 56$) Rydberg series of lithium versus the principal quantum number.

($14 \leqslant n \leqslant 56$) Rydberg series are listed in Table I. The n^* have been calculated using the Rydberg relation

$$n^* = \sqrt{\frac{R_{Li}}{V_{\text{ion}} - E_n}}, \tag{6}$$

where R_{Li} is the Rydberg constant of lithium, V_{ion} is the ionization potential, and E_n is the energy of the observed transition. The value of R_{Li} and V_{ion} are taken as 109 728.64 cm^{-1} and 43 487.26 cm^{-1} [46], respectively. The oscillator strengths are plotted against the principal quantum number n in Fig. 7. The solid line is the fit of Eq. (5) to the experimental data points indicating a smooth decrease of the f values as $n^{-2.83}$. The product $(n^{*3}f)$ verses the principal quantum number n is plotted in Fig. 8. The solid line is the linear fit to the measured values that shows an increasing trend. A similar behavior has been observed by Fillipove [5], and Marr and Greek [6] for the f values of the $2s \rightarrow np$ ($3 \leqslant n \leqslant 9$) Rydberg series of lithium, and may be due to the

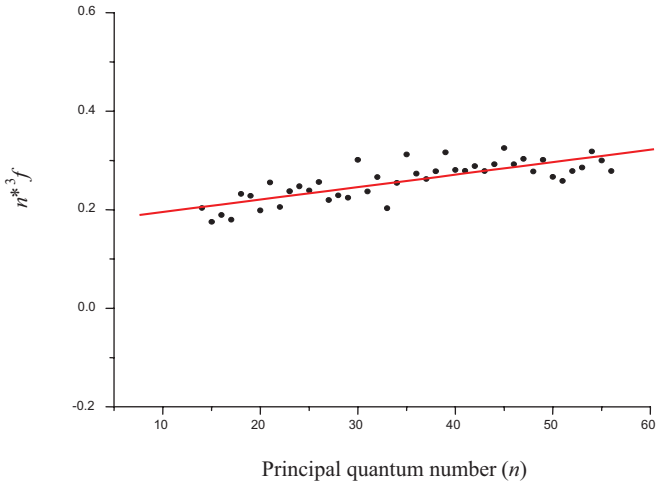

FIG. 8. (Color online) A plot of the $(n^*)^3 f$ corresponding to the transitions of the $3s\,^2S \rightarrow np\,^2P$ ($14 \leqslant n \leqslant 56$) Rydberg series of lithium versus the principal quantum number.

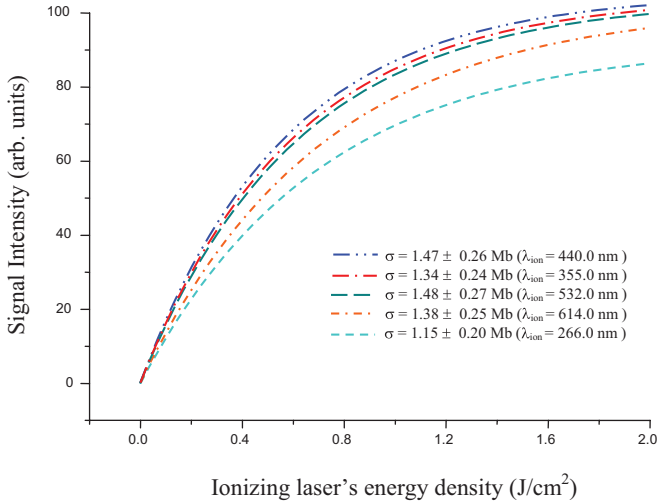

FIG. 9. (Color online) The fitted curves to the experimental data versus the energy density of the ionizing laser for the photoionization cross section from the $3s\ ^2S$ excited state of lithium at threshold (614 nm), at 532 nm, at 440 nm, at 355 nm, and at 266 nm. These fitted curves are used to extract the photoionization cross sections of the $3s\ ^2S$ excited state.

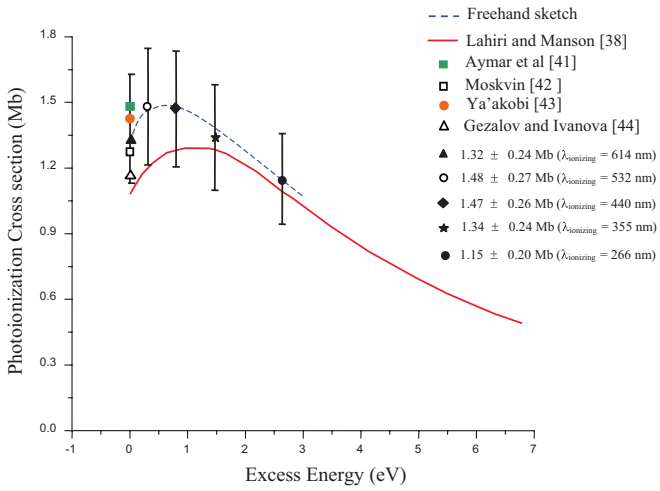

FIG. 10. (Color online) Comparison of the experimentally measured values of the absolute photoionization cross section from $3s\ ^2S$ excited state with the theoretical work. The solid line is the calculated curve presented by Lahiri and Manson [38]. The calculated values at threshold by Aymar *et al.* [41], Moskvin [42], Ya'akobi [43], and Gezalov and Ivanova [44] are also shown.

presence of the Cooper minima around $n=3$ [7]. We have determined the f values for the transitions of the $3s\ ^2S \rightarrow np\ ^2P$ series from $n=14$ to $n=56$ and did not observe the presence of any Cooper minima in this region.

Subsequently we extended the measurements of oscillator strengths from the discrete region to the ionization continuum. The oscillator strength f_n in the discrete spectrum merges into the differential oscillator strength df/dE in the continuous spectrum, which are related as [4]

$$\frac{(n^*)^3 f_n}{2R} = \frac{df}{dE}. \tag{7}$$

Here, n^* is the effective quantum number, R is the Rydberg constant, and E is the photon energy. The spectral density of the oscillator strength is also related to the photoionization cross section as [4]

$$\sigma(E) = 1.098 \times 10^{-16} \frac{df}{dE}\ \text{cm}^2\ \text{eV},$$

or

$$\frac{df}{dE} = 9.11 \times 10^{15}\ \sigma(E)\ \text{cm}^{-2}\ (\text{eV})^{-1}. \tag{8}$$

Therefore, to find the spectral density of the oscillator strengths corresponding to the $3s\ ^2S_{1/2}$ excited state we measured the photoionization cross section from the $3s$ excited state above the first ionization threshold at four ionizing laser wavelengths of 532 nm, 440 nm, 355 nm, and 266 nm, using the saturation technique [Eq. (3)]. Figure 9 shows the varia-

TABLE II. Experimental data for the absolute photoionization cross section from the $3s$ excited state of lithium.

	Present work			
State	Wavelength (nm)	Cross section (Mb)	$\left(\frac{df}{dE}\right)_\varepsilon$ (eV^{-1})	Previous work Cross section (Mb)
$3s\ ^2$S				1.48 (Ref. [41])
	614	1.32±0.24	0.01203±(20%)	1.27 (Ref. [42])
				1.42 (Ref. [43])
				1.17 (Ref. [44])
				1.42 (Ref. [45])
	532	1.48±0.27	0.01348±(20%)	
	440	1.47±0.26	0.01339±(%20)	
	355	1.34±0.26	0.01222±(20%)	
	266	1.15±0.20	0.01047±(20%)	

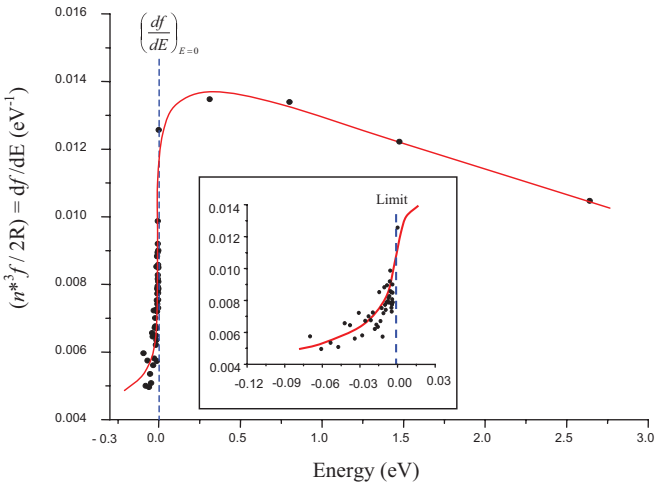

FIG. 11. (Color online) The experimentally measured oscillator strength distribution in the discrete and the continuous spectrum of lithium.

tion of the photoion signal with the laser intensity for the five ionizing lasers at threshold (614 nm), at 532 nm, at 440 nm, at 355 nm, and at 266 nm. Each curve is a least square fit of Eq. (3) to the experimental data points. The measured values of the photoionization cross section from this fitting procedure along with the earlier theoretical work are shown in Fig. 10. The continuous curve is the work of Lahiri and Manson [38] who used the Central-Potential Model to calculate the cross section of the excited states of lithium. The calculated values of the cross section for the 3*s* excited state, at the ionization threshold, is also shown in the Fig. 10. To our knowledge, no other measurements for the photoionization cross section of the 3*s* excited state of lithium has been reported in the literature.

The behavior of the photoionization cross section for the excited states can be correlated with the difference between the initial state quantum defect and the final continuum threshold phase shift [38,47,48]. There is only one channel εp through which the electrons from the *ns* excited states can be promoted to the ionization continuum. The difference between the ns quantum defect and the threshold εp phase shift is 0.37 for lithium, which indicates a minimum in the discrete region near threshold. The presence of this minimum causes the ns cross section to be anomalously small at threshold [38]. The measured values of the photoionization cross section from the $3s\ ^2S$ excited state are 1.32 Mb, 1.48 Mb, 1.47 Mb, 1.34 Mb, and 1.15 Mb at threshold and at excess photon energies of 0.3 eV, 0.8 eV, 1.5 eV, and at 2.6 eV respectively above threshold. It is apparent that the photoionization cross section from the 3*s* excited state at the ionization threshold is lower than its value at 0.3 eV excess energy. The dashed line in Fig. 10 is a freehand sketch to show the energy dependent trend of the measured photoionization cross section. Evidently, the photoionization cross section first increases to a maximum value (1.48 Mb) and then decreases with the decrease in the ionizing laser wavelength deviating from the hydrogenic behavior. This confirms the theoretical prediction of Lahiri and Manson [38] about the behavior of the cross sections of the *ns* excited states of lithium.

The density of oscillator strength were then determined from the measured values of the photoionization cross section, using Eq. (8), at the excess photon energies of 0.3 eV, 0.8 eV, 1.5 eV, and 2.6 eV above the first ionization threshold, and are tabulated in Table II. To give an overall view of the oscillator strength distribution of the lithium spectrum, in Fig. 11 we have plotted on the same graph the oscillator strengths f_n in the discrete spectrum and the related oscillator strength density df/dE in the continuum. The solid line is a free hand sketch to the experimental data points just to guide the trend of the oscillator strength distribution in the discrete and in the continuum regions while the dashed line represents the ionization threshold. This figure clearly indicates the merging of the discrete absorption features with the continuous absorption at the ionization threshold. The inset in the figure shows an expanded view of the discrete region from the threshold up to −0.12 eV. Our data suggests that if a Cooper minimum is present, it must lie between the $n=4$ and $n=13$ excitations as our oscillator strengths are monotonically increasing above $n=14$.

The maximum overall uncertainty in the determination of the absolute photoionization cross section is estimated to be 18% [49], which is attributed to the experimental errors in the measurements of the laser energy, the cross-sectional area of the laser beam at the focusing volume, the calibration of the detection system and a non-uniform transmission of the quartz windows. The uncertainty in the measurements of the *f*-values is about 20%, which is attributed to additional errors in the measurements of the laser energy and transition width measurements.

In conclusion, we have experimentally determined the oscillator strength distribution both in the discrete and in the continuous spectrum starting from the $3s\ ^2S$ excited state of lithium for the first time. Continuity across the ionization threshold has been found. This technique can be extended to determine the oscillator strength distribution in the discrete and the continuous spectra of all the alkali and the alkaline earth elements. Further work in this direction is in progress in our laboratory.

ACKNOWLEDGMENTS

The present work was financially supported by the Higher Education Commission (HEC), Pakistan Science Foundation (PSF), and the Quaid-i-Azam University, Islamabad, Pakistan.

[1] U. Fano and J. W. Cooper, Rev. Mod. Phys. **40**, 441 (1968).
[2] G. W. F. Drake, *Atomic, Molecular, & Optical Physics Handbook* (AIP Press, New York, 1996).
[3] M. C. E. Huber and R. J. Sandeman, Rep. Prog. Phys. **49**, 397 (1986).
[4] J. Berkowitz, *Photoabsorption, Photoionization and Photoelectron Spectroscopy* (Academic Press, New York, 1979); *Atomic and Molecular Photoabsorption, Absolute Total Cross Sections* (Academic Press, New York, 2002).
[5] A. N. Filippov, Z. Phys. **69**, 526 (1931).
[6] G. V. Marr and D. M. Greek, Proc. - R. Soc. Edinburgh, Sect. A: Math. **304**, 245 (1968).
[7] W. L. Wiese and A. W. Wiese, Phys. Rev. **175**, 50 (1968).
[8] G. A. Martin and W. L. Wiese, Phys. Rev. A **13**, 699 (1976).
[9] G. A. Martin and W. L. Wiese, J. Phys. Chem. Ref. Data **5**, 537 (1976).
[10] J. S. Sims, S. A. Hagstrom, and J. R. Rumble Jr., Phys. Rev. A **13**, 242 (1976).
[11] M. Y. Amusia and N. A. Cherepkov, Phys. Rev. A **13**, 1466 (1976).
[12] D. Hofsaess, Z. Phys. A **281**, 1 (1977).
[13] I. Martin and C. Barrientos, Can. J. Phys. **64**, 867 (1986).
[14] C. Barrientos and I. Martin, Can. J. Phys. **65**, 435 (1987).
[15] C. Barrientos and I. Martin, Can. J. Phys. **67**, 996 (1989).
[16] G. Peach, H. E. Saraph, and M. J. Seaton, J. Phys. B **21**, 3669 (1988).
[17] C. Barrientos and I. Martin, Phys. Rev. A **42**, 432 (1990).
[18] E. Hollauer and Marco Antonio Chaer Nascimento, Phys. Rev. A **42**, 6608 (1990).
[19] C. F. Fischer, Nucl. Instrum. Methods Phys. Res. B **31**, 265 (1988).
[20] A. W. Weiss, Can. J. Chem. **70**, 456 (1992).
[21] M. Tong, P. Jonsson, and C. F. Fischer, Phys. Scr. **48**, 446 (1993).
[22] Z. C. Yan and G. W. F. Drake, Phys. Rev. A **52**, R4316 (1995).
[23] R. N. Barnett, E. M. Johnson, and W. A. Lester, Jr., Phys. Rev. A **51**, 2049 (1995).
[24] L. Qu, Z. Wang and B. Li, Eur. Phys. J. D **5**, 173 (1999).
[25] D. Hanna, P. A. Karkainen, and R. Wyatt, Opt. Quantum Electron. **7**, 115 (1975).
[26] G. R. Harrison, *M. I. T. Wavelength Tables* (M.I.T. Press, England, 1982).
[27] W. Mende and M. Kock, J. Phys. B **29**, 655 (1996).
[28] C. E. Burkhardt, J. L. Libbert, Jian Xu, J. J. Leventhal, and J. D. Kelley, Phys. Rev. A **38**, 5949 (1988).
[29] L. W. He, C. E. Burkhardt, M. Ciocca, J. J. Leventhal, and S. T. Manson, Phys. Rev. Lett. **67**, 2131 (1991).
[30] M. Saleem, Shahid Hussain, M. Rafiq, and M. A. Baig, J. Phys. B **39**, 5025 (2006).
[31] N. Amin, S. Mahmood, M. Anwar-ul-Haq, M. Riaz, and M. A. Baig, Eur. Phys. J. D **37**, 23 (2006).
[32] Shahid Hussain, M. Saleem, M. Rafiq, and M. A. Baig, Phys. Rev. A **74**, 022715 (2006).
[33] M. Saleem, N. Amin, S. Hussain, M. Rafiq, S. Mahmood, and M. A. Baig, Eur. Phys. J. D **38**, 277 (2006).
[34] S. Mahmood, N. Amin, Sami-ul-Haq, N. M. Shaikh, S. Hussain, and M. A. Baig, J. Phys. B **39**, 2299 (2006).
[35] S. Hussain, M. Saleem, and M. A. Baig, Phys. Rev. A **74**, 052705 (2006).
[36] W. Demtroder, *Laser Spectroscopy* (Springer Verlag, Berlin, 1996).
[37] J. M. Song, T. Inoue, H. Kawazumi, and T. Ogawa, Anal. Sci. **15**, 601 (1999).
[38] J. Lahiri and S. T. Manson, Phys. Rev. A **48**, 3674 (1993).
[39] K. Niemax, Appl. Phys. B **38**, 147 (1985).
[40] V. Svedas, J. Phys. B **21**, 301 (1988).
[41] M. Aymar, E. Luc-Koenig, and F. C. Farnoux, J. Phys. B **9**, 1279 (1976).
[42] Yu. V. Moskvin, Opt. Spectrosc. **15**, 316 (1963).
[43] B. Ya'akobi, Proc. Phys. Soc. London **92**, 100 (1967).
[44] K. B. Gezalov and A. V. Ivanova, High Temp. **6**, 400 (1968).
[45] T. C. Caves and A. Dalgarno, J. Quant. Spectrosc. Radiat. Transf. **12**, 1539 (1972).
[46] M. Anwar-ul-Haq, S. Mahmood, M. Riaz, R. Ali, and M. A. Baig, J. Phys. B **38**, S77 (2005).
[47] J. Lahiri and S. T. Manson, Phys. Rev. A **33**, 3151 (1986).
[48] Z. Felfli and S. T. Manson, Phys. Rev. A **41**, 1709 (1990).
[49] J. Topping, *Errors of Observation and Their Treatment* (Chapman and Hall, London, 1962).